Conformation-specific inhibitors of activated Ras GTPases reveal limited Ras dependency of patient-derived cancer organoids

Received for publication, September 11, 2019, and in revised form, February 18, 2020 Published, Papers in Press, February 20, 2020, DOI 10.1074/jbc.RA119.011025

Svenja Wiechmann,[a,b] Pierre Maisonneuve,[c1] Britta M. Grebbin,[d,e,f] Meike Hoffmeister,[a,g] Manuel Kaulich,[a,h] Hans Clevers,[i,j,k] Krishnaraj Rajalingam,[l2] Igor Kurinov,[m] Henner F. Farin,[d,e,f] Frank Sicheri,[c3] and Andreas Ernst[a,b4]

From the [a]Institute of Biochemistry II, Goethe University Frankfurt–Medical Faculty, University Hospital, 60596 Frankfurt am Main, Germany, the [b]Fraunhofer Institute for Molecular Biology and Applied Ecology IME, Project Group Translational Medicine and Pharmacology TMP, Theodor-Stern-Kai 7, 60590 Frankfurt am Main, Germany, the [c]Lunenfeld-Tanenbaum Research Institute, Sinai Health System, Toronto, Ontario M5G 1X5, Canada, the [d]German Cancer Consortium (DKTK), 69120 Heidelberg, Germany, the [e]Georg-Speyer-Haus, Institute for Tumor Biology and Experimental Therapy, 60596 Frankfurt am Main, Germany, the [f]German Cancer Research Center (DKFZ), 69120 Heidelberg, Germany, the [g]Institute of Biochemistry, Brandenburg Medical School (MHB) Theodor Fontane, 14770 Brandenburg an der Havel, Germany, the [h]Frankfurt Cancer Institute, 60596 Frankfurt am Main, Germany, the [i]Hubrecht Institute, Royal Netherlands Academy of Arts and Sciences (KNAW) and University Medical Center Utrecht, 3584 CX Utrecht, The Netherlands, [j]Cancer Genomics Netherlands, University Medical Center Utrecht, 3584 CX Utrecht, The Netherlands, the [k]Center for Molecular Medicine, Department of Genetics, University Medical Center Utrecht, 3584 CX Utrecht, The Netherlands, the [l]Cell Biology Unit, University Medical Center Mainz, JGU-Mainz, 55131 Mainz, Germany, and the [m]Department of Chemistry and Chemical Biology, Cornell University, NE-CAT, Argonne, Illinois 60439

Edited by Alex Toker

The small GTPases H, K, and NRAS are molecular switches indispensable for proper regulation of cellular proliferation and growth. Several mutations in the genes encoding members of this protein family are associated with cancer and result in aberrant activation of signaling processes caused by a deregulated recruitment of downstream effector proteins. In this study, we engineered variants of the Ras-binding domain (RBD) of the C-Raf proto-oncogene, Ser/Thr kinase (CRAF). These variants bound with high affinity with the effector-binding site of Ras in an active conformation. Structural characterization disclosed how the newly identified RBD mutations cooperate and thereby enhance affinity with the effector-binding site in Ras compared with WT RBD. The engineered RBD variants closely mimicked the interaction mode of naturally occurring Ras effectors and acted as dominant-negative affinity reagents that block Ras signal transduction. Experiments with cancer cells showed that expression of these RBD variants inhibits Ras signaling, reducing cell growth and inducing apoptosis. Using these optimized RBD variants, we stratified patient-derived colorectal cancer organoids with known Ras mutational status according to their response to Ras inhibition. These results revealed that the presence of Ras mutations was insufficient to predict sensitivity to Ras inhibition, suggesting that not all of these tumors required Ras signaling for proliferation. In summary, by engineering the Ras/Raf interface of the CRAF-RBD, we identified potent and selective inhibitors of Ras in its active conformation that outcompete binding of Ras-signaling effectors.

The small GTPases HRAS, KRAS, and NRAS are molecular switches that relay signals from growth factor receptor tyrosine kinases to transcription factors and other intracellular mediators to affect the growth, proliferation, and survival of cells. To achieve this function, the conformation of Ras GTPases cycles between an inactive, GDP-bound state and an active, GTP-bound state that interacts with downstream effector proteins. Along this reaction cycle, the weak hydrolysis activity of Ras is enhanced by GTPase-activating proteins, and guanine exchange factors facilitate the discharge of GDP and the reloading with GTP. In cancer, mutations in members of the Ras family shift the fine-tuned equilibrium of this reaction cycle toward the active, GTP-bound state, leading to a constitutive activation of downstream kinases. The resulting uncoupling of the regulatory link between proliferation and upstream receptor signaling leads to uncontrolled growth and proliferation. Thus, mutated Ras GTPases are oncogenic drivers in various malignancies, making them, and their downstream effector kinases, a major focus for the development of antiproliferative drugs.

When in active conformation, Ras GTPases propagate signals by the recruitment of kinases of the Raf family, thereby

This work was supported by LOEWE Ub-Net, Cluster of Excellence "Macromolecular Complexes" (DFG EXC115) and the Collaborative Research Center SFB 1177. This work was also supported by funds from Impact Grant 704116 (to F. S.) from the Canadian Cancer Society Research Institute and by operating fund Grant FDN143277 (to F. S.) from the Canadian Institutes for Health Research. The authors declare that they have no conflicts of interest with the contents of this article. The content is solely the responsibility of the authors and does not necessarily represent the official views of the National Institutes of Health.

This article contains Tables S1–S5 and Figs. S1–S5.

[1]Supported by a TD Bank postdoctoral fellowship.

[2] A Heisenberg professor of the DFG (Grant RA1739/4-2).

[3] Holder of a Canada Research Chair (Tier 1) in Structural Biology of Cell Signaling.

[4] To whom correspondence should be addressed: Institute of Biochemistry II, Goethe University Frankfurt–Medical Faculty, University Hospital, Frankfurt am Main, Germany. E-mail: ernst2001@gmail.com.

stimulating growth factor–signaling pathways (1). Members of this family of kinases interact with several different GTPases of the Ras subfamily. For example, BRAF is activated by oncogenic Ras and by the GTPase Rap1 (2, 3). In a two-hybrid assay, the kinases ARAF and CRAF interact with the closely Ras-related GTPase RRAS (4). Furthermore, the CRAF Ras-binding domain (RBD)[5] crystallized in complex with either HRAS or RAP1A, indicating that both interactions are sufficiently strong to yield co-crystal structures (5, 6). This multispecificity of Raf kinases relates to the conservation of the effector-binding site and RBD at the atomic molecular level (7). Thus, reagents that interfere with the Ras/Raf interaction are likely to efficiently inhibit the activation of growth signals over a wide range of conditions.

Developing inhibitors of Ras has been challenging because of the high affinity of GDP/GTP for the GTP-binding pocket of the Ras family of GTPases and due to the flat topology of the conserved effector-binding site (8, 9). Consequently, to date, only a few small-molecule inhibitors exist that directly interfere with Ras function (10). To overcome the paucity of small molecules that directly interfere with Ras activity, several affinity reagents based on protein scaffolds have been developed to address different facets of Ras biology. For example, fibronectin-derived monobodies inhibit signaling by disrupting the dimerization of HRAS and KRAS at the plasma membrane (11). Interfering with Ras dimerization limits the growth of xenografts that inducibly express the monobody (12). An alternative strategy for inhibiting Ras signaling with engineered proteins is to prevent the recruitment of downstream effectors or block the activation of Ras by guanine exchange factors. To this end, affinity reagents have been generated that compete with Ras effectors by selectively binding to the active or inactive state of oncogenic Ras (13–19). However, several require high concentrations to be effective in cells (16, 17, 20), and their selectivity for members of the Ras family is unknown. The limited effectiveness may be related to the interaction of Raf-family kinases with various Ras GTPases. Thus, a rationale for affinity reagents with improved efficacy could be those that block interactions with multiple Ras family members simultaneously.

An ideal affinity reagent that inhibits Ras function should precisely replicate the spatial constraints of effector binding to activated, GTP-bound Ras. Additionally, these affinity reagents should have a high affinity with the effector-binding site and the ability to outcompete downstream effectors. Consequently, such an affinity reagent would act as an inhibitor of Ras signaling, which could be used to probe the biology of Ras inhibition in cellular and patient-derived model systems. To derive an affinity reagent that fulfills these criteria, we adapted our strategy of optimizing pre-existing intermolecular contacts (21, 22) to the RBD of CRAF. We constructed a phage-displayed RBD library encoding mutations of interface residues and selected for improved binding to active, GTP-bound Ras. Crystal structures of complexes with activated HRAS G12V showed that the RBD variants (RBDvs) precisely mimic effector binding, and the engineered mutations subtly improve intermolecular contacts. Importantly, intracellular expression of individual RBDvs resulted in impaired growth of various cancer cell lines due to a robust inhibition of Ras signaling and the MAPK signaling cascade. Finally, in patient-derived colorectal cancer organoids with mutant or WT Ras status, we observed differential effects of the RBDvs on cellular growth and metabolic activity. These results indicate that not all tumors are equally dependent on Ras signaling to sustain a proliferative phenotype and that genetic data alone are insufficient to predict responsiveness to Ras inhibition. The ability of the RBDvs to inhibit growth of cells lacking activating mutations in Ras family members may relate to their multispecificity in interacting with active conformations of Ras GTPases with a conserved switch-1 region.

Results

Engineered RBD variants have high affinity for GTP-bound Ras and compete with effector binding in vitro

Previous studies demonstrated that the CRAF-RBD is highly tolerant to mutations and can be computationally engineered to preferentially bind inactive states of Ras (18, 23, 24). To optimize the interface of the RBD to active Ras, we analyzed existing crystal structures of Ras:RBD complexes (5, 25, 26). In total, we identified 14 residues that make side-chain contacts to the switch-1 region of the Ras effector-binding site. These residues are located on the $\beta1$-$\beta2$ hairpin and $\alpha1$ helix and span two distinct regions of the CRAF-RBD. To achieve a moderate to low mutation rate that does not alter the binding mode or impair the structure of the RBD, we used a randomization strategy that allowed 70% of the WT nucleotides and 10% of the non-WT nucleotides to occur at any codon position encoding the targeted residues (Fig. 1*A*). Such a randomization approach results in a high probability of WT residues at the targeted positions and is commonly referred to as soft randomization. Additionally, we replaced three unpaired cysteines at positions 81, 95, and 96 of the RBD with serine residues to prevent dimerization of phage-displayed proteins and improve overall presentation of the RBDvs. Our final library contained more than 2×10^9 unique RBDvs presented on the surface of filamentous phage, and subsequent selection by phage display yielded five variants with improved binding to surface-immobilized GTPγS-loaded HRAS (Fig. 1*B*). The selected variants show a conserved mutational pattern, indicating a shared binding mode to activated Ras. Strikingly, the mutation of Gln^{66} to Glu is highly enriched in all five variants, indicating that this mutation has a crucial role in mediating the increased affinity. Coincidentally, the mutation from Val^{88} to Arg, previously shown to

[5] The abbreviations used are: RBD, Ras-binding domain; RBDv, RBD variant; RBDwt, WT RBD; MAP, GNP, phosphoaminophosphonic acid-guanylate ester; MAPK, mitogen-activated protein kinase; GTPγS, guanosine 5′-3-*O*-(thio)triphosphate; RA, Ras association domain; RalGDS, Ral guanine nucleotide dissociation stimulator; MS, mass spectrometry; HA, hemagglutinin; MEK, mitogen-activated protein kinase/extracellular signal-regulated kinase kinase; ERK, extracellular signal–regulated kinase; CRC, colorectal cancer carcinoma; DARPin, designed ankyrin repeat protein; AA, amino acids; PMSF, phenylmethylsulfonyl fluoride; TEV, tobacco etch virus; TCEP, tris(2-carboxyethyl)phosphine; SEC, size-exclusion chromatography; GMP-PNP, 5′-guanylylimidodiphosphate; PDB, Protein Data Bank; GAPDH, glyceraldehyde-3-phosphate dehydrogenase; AGC, automatic gain control; HRP, horseradish peroxidase; RTCA, real-time cell analysis; DOX, doxycycline; PI3K, phosphatidylinositol 3-kinase; EGF, epidermal growth factor.

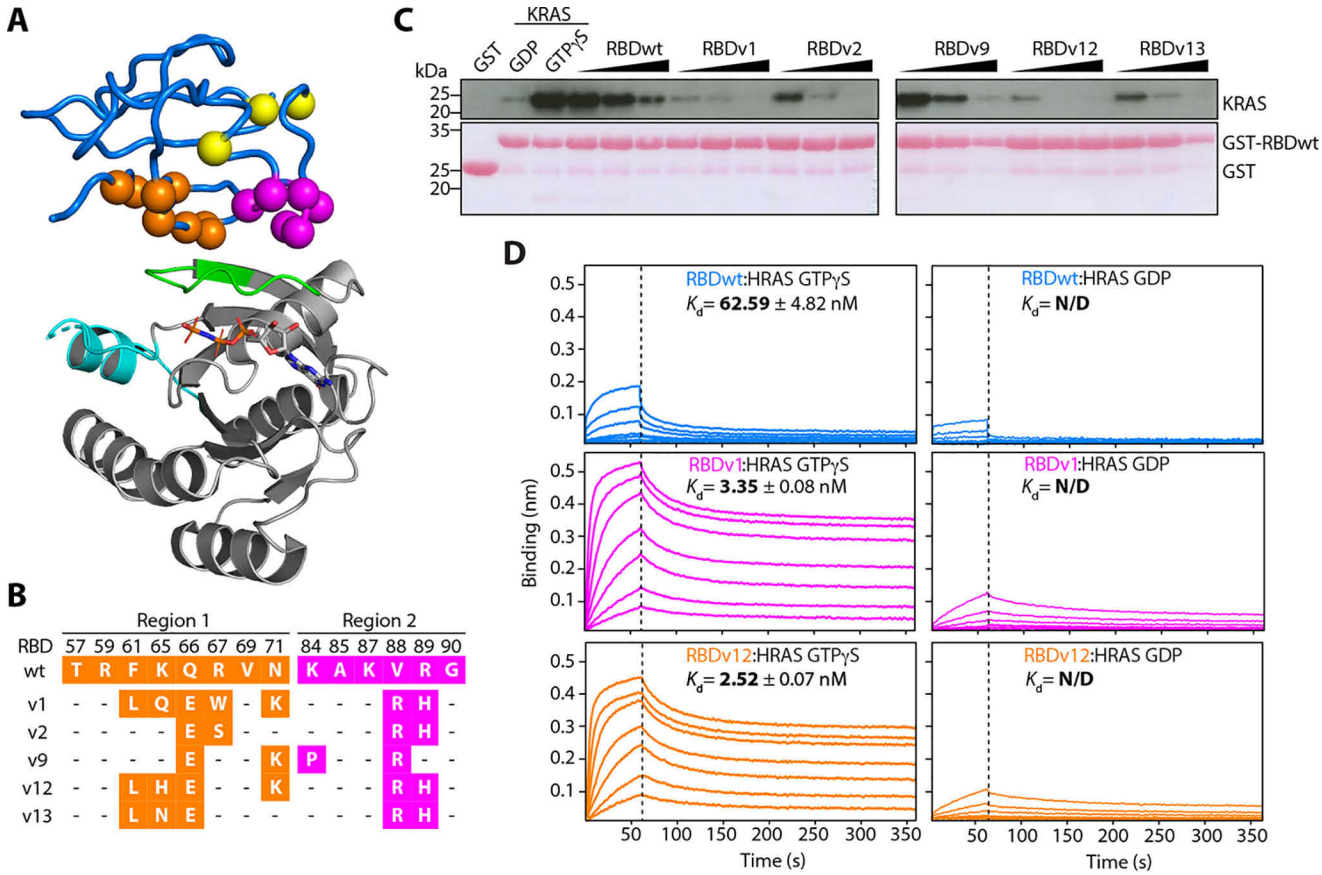

Figure 1. CRAF-RBD library design and selected RBDvs outcompete RBDwt by binding with highly improved affinity to active Ras. *A*, CRAF-RBD in complex with HRAS (PDB entry 4G0N) (5). The RBD is shown as a *blue tube*, and HRAS is shown as a *gray ribbon*, indicating the location of switch-1 (*green*) and switch-2 (*cyan*). Bound GTP analog GNP is shown as *sticks*. Residues modified in region 1 (*orange*) and region 2 (*magenta*) and Cys to Ser mutations (*yellow*) of CRAF-RBD are shown as *colored spheres*. *B*, sequences of RBDvs selected by phage display. Residues in region 1 and region 2 are *colored* as in *A*. Nonmutated positions are indicated by *dashes*. *C*, *in vitro* competition of His-tagged GTPγS-loaded KRAS binding to GST-tagged RBDwt immobilized on GSH Sepharose resin with increasing molar ratios of His-tagged RBDvs or RBDwt (1:1, 1:2.5, and 1:10). KRAS bound to beads was detected by immunoblotting, and the corresponding Ponceau S–stained membrane is shown. *D*, binding of GTPγS- and GDP-loaded HRAS to immobilized GST-tagged RBDwt (*blue*), RBDv1 (*magenta*), or RBDv12 (*orange*) measured by bio-layer interferometry. Concentrations of Ras ranged from 1 μM to 15.6 nM in a 1:1 dilution series. K_d values for each experiment are shown.

increase the affinity of RBD to HRAS (27), was also present in all five variants. An Arg^{89} to His mutation occurred in four of the five RBDvs.

After purification as His-tagged proteins, we tested whether the engineered RBDvs outcompeted CRAF-RBDwt binding to GTPγS-loaded KRAS *in vitro* (Fig. 1*C*). Relative to RBDwt, all engineered variants showed an enhanced ability to compete off GTPγS KRAS in solution. A similarly enhanced competitive ability of the RBDvs was observed using the Ras association domain (RA) of Ral guanine nucleotide dissociation stimulator (RalGDS) instead of the CRAF-RBDwt (Fig. S1*A*). Because RBDv1 and RBDv12 performed best in these experiments, we focused our further analysis on these two variants.

Affinity measurements confirmed that RBDv1 and RBDv12 have an up to 20-fold improved binding to activated, GTPγS-loaded HRAS relative to RBDwt with negligible binding to the GDP-bound form (Fig. 1*D*). In control experiments, we verified that His-tagged HRAS GTPγS does not bind to GST-loaded sensors or empty sensors alone (Fig. S1*B*), indicating that the slow off rate is not due to nonspecific binding of HRAS to GST or the sensor material.

The engineered RBDvs mimic effector binding to active Ras

To understand the structural basis for improved binding, we crystallized GMP-PNP–bound HRAS G12V in complex with RBDv1 at 2.9 Å and RBDv12 at 3.15 Å resolution in an active conformation (Fig. 2*A* and Table S1). Representative electron density of both structures at the binding interface is shown in Fig. S2*A*. Structural analysis revealed that the RBDvs engaged the effector-binding site of HRAS through a canonical binding mode (5) with only minor shifts to the center of mass positions and rotation angle (1.8 Å/15° and 2.0 Å/16° for RBDv1 and RBDv12, respectively). Similar to the canonical binding mode of RBDwt, β2 of the RBDvs forms an extended intermolecular β-sheet with β2 of HRAS (Fig. S2*B*). In addition, helices α1 of both RBDwt and RBDvs form direct contacts with switch-1 residues in Ras (Fig. 2*A*). Binding of RBDwt to HRAS is mediated by a mixture of 24 hydrogen-bond and salt-bridge interactions, whereas binding of RBDv1 and RBDv12 with HRAS is mediated by a mixture of 14 hydrogen-bond and salt-bridge interactions (Table S2). Only two interactions, namely those between RBD Thr^{68} and Val^{89} and HRAS Asp^{38} and Glu^{37}, respectively, are common in the three structures. Inspection of the direct contact interface reveals that the conserved RBDv

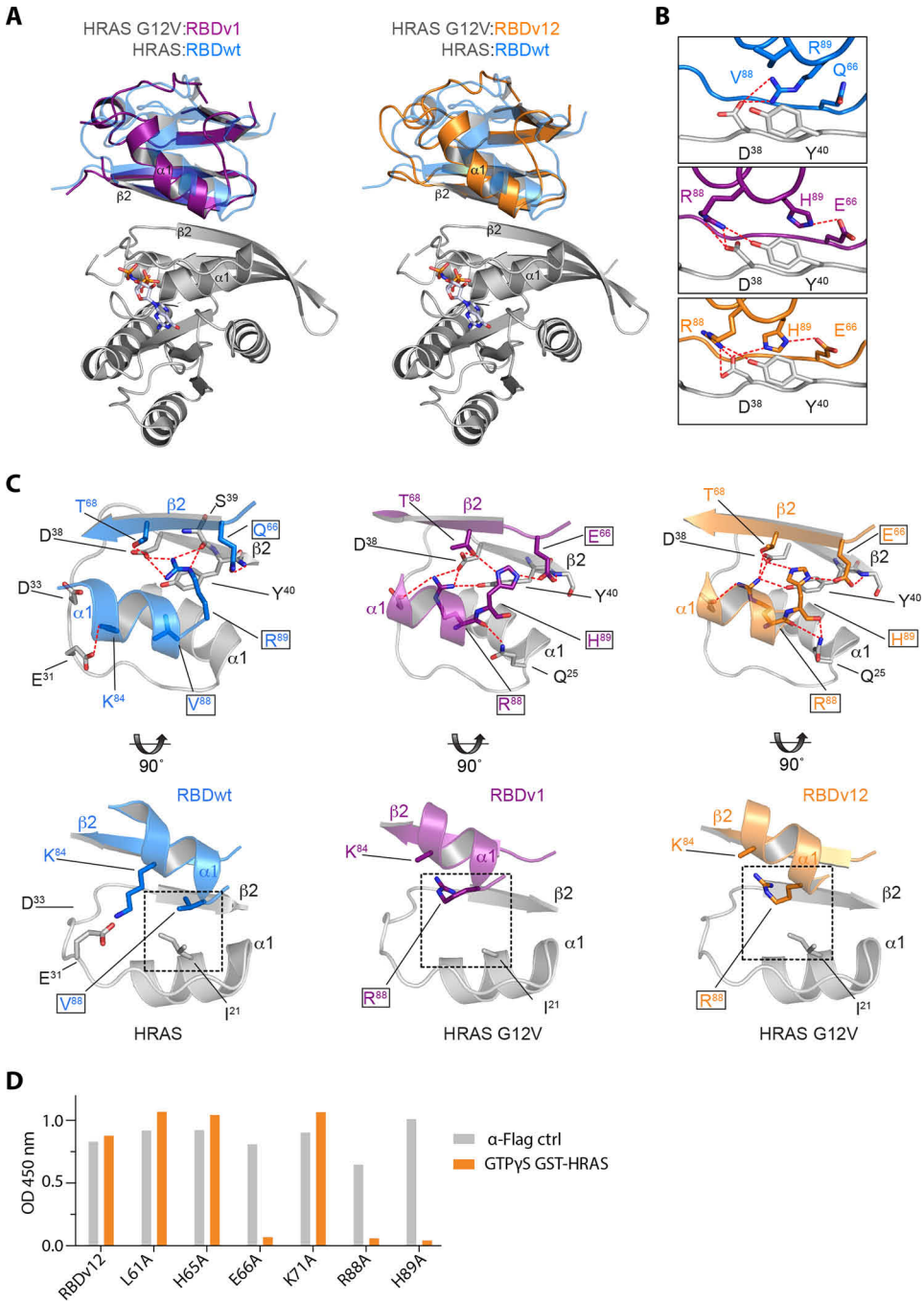

Figure 2. RBDvs bind at the Ras effector-binding site. *A*, crystal structures of HRAS G12V (*gray*) in complex with RBDv1 (*magenta*) at 2.9 Å or RBDv12 (*orange*) at 3.15 Å resolution. Both structures are superimposed on HRAS in complex with RBDwt (*blue*) (PDB code 4G0N) (5). For clarity, only HRAS G12V and the GTP analog GNP are shown as *colored sticks*. *B*, side-by-side comparison of HRAS in complex with RBDwt (*top*), RBDv1 (*middle*), or RBDv12 (*bottom*) showing changes caused by mutations at positions 66, 88, and 89. Polar interactions are indicated by *dashed lines* (*red*). HRAS G12V, RBDwt, RBDv1, and RBDv12 main and side chains are *colored* as in *A*. Residues are *numbered* according to the PDB entry for 4G0N. *C*, *top* and *side view* of the binding interface of RBDwt and RBDvs with HRAS. Residues involved in intermolecular interactions are shown as *sticks*. Residues that are mutated in RBDvs are *highlighted* by a *black square*. The *90° rotated side view* highlights the steric clash between Ile^{21} in HRAS and Val^{88} to Arg in RBDvs that is involved in a shift of the α1-helix of the RBDvs relative to that observed in RBDwt. *D*, binding of phage-displayed RBDv12 and RBDv12 alanine mutations to immobilized GTPγS-loaded GST-tagged HRAS (*orange*) or anti-FLAG antibody control (*gray*) measured by ELISA.

mutations of Gln^{66} to Glu, Val^{88} to Arg, and Arg^{89} to His result in the rewiring of the hydrogen-bonding and salt-bridge pattern to the Asp^{38} and Tyr^{40} side chains in HRAS (Fig. 2*B* and Table S2). This change in hydrogen-bonding pattern together with steric effects involving Ile^{21} in HRAS and Val^{88} to Arg in RBDvs appears responsible for a shift of the α1-helix of the RBDvs relative to that observed in RBDwt (Fig. 2*C*). Although unlikely, we cannot rule out that the different binding mode observed between the RBDvs compared with the RBDwt with HRAS is due to different crystal packing.

To test our hypothesis that the mutations at positions 66, 88, and 89 work together to improve binding, we performed a mutation analysis based on RBDv12 by replacing the engineered residues one by one with alanine. These alanine mutants

of RBDv12 were displayed on phage and probed for binding to active HRAS (Fig. 2*D*). This experiment provides evidence that replacement of Glu^{66}, Arg^{88}, or His^{89} in RBDv12 with alanine abolished binding to activated HRAS, indicating that all three residues are required to mediate binding. This loss of binding is most likely due to a perturbation of the hydrogen bond pattern at the interface caused by the aliphatic side chain of alanine in one of the positions. In summary, our combinatorial approach to RBD-interface engineering identified three key mutations that work together to improve contacts to residues in the switch-1 region of Ras in an active conformation. Because the binding mode of RBDvs to HRAS overlaps completely with RBDwt, the RBDvs are expected to outcompete binding of Ras effectors that engage this common binding site.

The RBDvs bind Ras GTPases in cells

We tested the intracellular specificity of the RBD variants using mass spectrometry (MS). We immunoprecipitated hemagglutinin (HA)-tagged RBDvs and HA-RBDwt that were inducibly expressed in stably transduced colon carcinoma HCT 116 cells (Fig. S3, *A* and *B*). HCT 116 cells are heterozygous for the activating mutant KRAS G13D. Strikingly, relative to RBDwt, RBDv1 and RBDv12 displayed up to 5500-fold enrichment of peptides from endogenous KRAS4B G13D isoform (Fig. 3*A* and Table S3). The prevalence of peptides originating from the constitutively active KRAS4B G13D isoform suggests that the RBDvs preferentially interact with Ras GTPases, which are in an active conformation.

We also detected peptides from other Ras-family GTPases, although these were ~10-fold less abundant than KRAS4B G13D peptides. Analysis of the primary sequences of the other Ras family members that interacted with the RBDvs showed that these Ras family members share a common effector-binding site (Fig. 3*B*). In particular, the detected peptides were from Ras family members containing Asp^{38} and Tyr^{40} residues in their respective switch-1 region, which we identified as key interaction residues for the RBDvs (Fig. 2*B*). Thus, the immunoprecipitation data showed that RBDvs bind to their intended targets, Ras proteins, in cells and exhibit the highest affinity for active Ras.

Consequently, these results suggested that the RBDvs are dominant-negative affinity reagents that will impair not only signaling through constitutive active Ras mutants but also other Ras GTPases in the active conformation. Thus, the RBDvs have the potential to inhibit multiple Ras-mediated pathways to Raf activation. Furthermore, the simultaneous inhibition of multiple Ras GTPases is potentially an efficient way to control the proliferation of cells with heterozygous KRAS genotypes, which confer resistance to MEK inhibitors (28).

RBDvs inhibit activation of the ERK and AKT pathways, resulting in reduced metabolic activity and apoptosis

To test whether the RBDvs act as inhibitors of Ras-dependent signaling processes, we probed whole-cell lysates from cell lines expressing HA-tagged RBDvs or RBDwt with antibodies detecting the phosphorylation state of kinases downstream of Ras proteins. We examined the effect of inhibition of Ras/Raf interaction on cell lines with different cancer origins and different Ras mutations at positions Gly^{12}, Gly^{13}, and Gln^{61} (Table S4). Specifically, cell lines with less frequent Ras mutations were chosen, because the crystal structures of the RBDvs in complex with HRas G12V already implied that the effector-binding site of Ras G12V would be inhibited by the RBDvs. Indeed, immunoblot analysis showed that the RBDvs reduced the phosphorylation of the growth signal–activated ERK1/2 in HCT 116, Mia PaCa-2, A549, and H1299 cells (Fig. 4*A*). The corresponding control experiments with RBDwt, despite its higher expression, did not reduce ERK1/2 phosphorylation, indicating that the improved affinity of the RBDvs for active Ras isoforms is required to suppress activation of these downstream kinases.

Reduced activity of the MAPK pathway often results in reduced cell viability. Therefore, we measured ATP content, as an indicator of metabolic activity and viability, and monitored growth curves, as an indicator of proliferation. In all four cell lines, inhibition of effector binding to active Ras by the RBDvs reduced cell viability (ATP content) (Fig. 4*B*), indicating that the RBDvs disrupt Ras signaling in cells from different cancer backgrounds. Importantly, RBDwt control had only minimal effects on the viability of all four cell lines. Five-day growth curves measured with HCT 116 cells confirmed that the RBDvs, but not RBDwt, inhibited proliferation (Fig. 4*C*).

Not only does Ras signaling mediate proliferative responses, but these GTPases also promote cell survival. In the presence of the RBDvs, HCT 116 cells exhibited reduced phosphorylation of Ser^{473} in the serine/threonine kinase AKT, indicating that the PI3K pathway is inhibited (Fig. 4*D*). Together, the reduced MAPK and PI3K pathway activity could not only reduce cellular metabolic activity and proliferation but could also increase apoptosis. We monitored HCT 116 cells expressing either RDBvs or RBDwt for annexin V staining as an indicator of apoptotic cells (Fig. 4*E* and Fig. S4). Quantification of annexin V staining by flow cytometry revealed that HCT 116 cells expressing the RBDvs had a significantly increased number of apoptotic cells compared with noninduced controls and compared with induced cells expressing RBDwt. In summary, these results showed that the RBDvs inhibit the ERK and PI3K signaling pathway, resulting in growth reduction in a wide range of cancer cell lines and inducing apoptosis in HCT 116 cells.

RBDvs lead to reduced growth in patient-derived colorectal cancer organoids

To investigate whether the characteristics of our RBDvs in cell culture can be translated into a patient-derived model, we used tumor organoids with known Ras mutation status isolated from surgically removed colorectal carcinoma from seven patients (29) (Table 1 and Table S5). After transduction with the doxycycline-inducible lentiviral constructs, we compared cell viability and growth of organoids, cultured in Matrigel and expressing RBDvs or RBDwt. We evaluated by immunoblot of organoid lysates ERK and AKT phosphorylation in response to doxycycline-induced expression of the RBDvs or RBDwt (Fig. 5*A* and Fig. S5*A*). The different organoids showed different sensitivity to the inhibitory effects of the RBDvs on these two kinases. For example, P17T with WT KRAS showed little effect of RBDv12, and P6T with KRAS G12C showed a stronger effect of the RBDvs on ERK1/2 phosphorylation than on AKT phos-

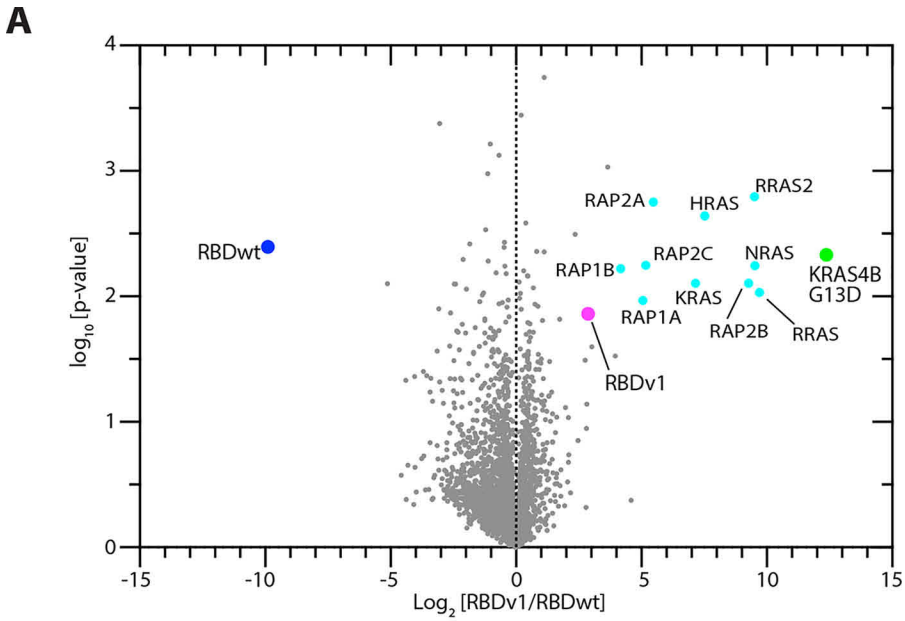

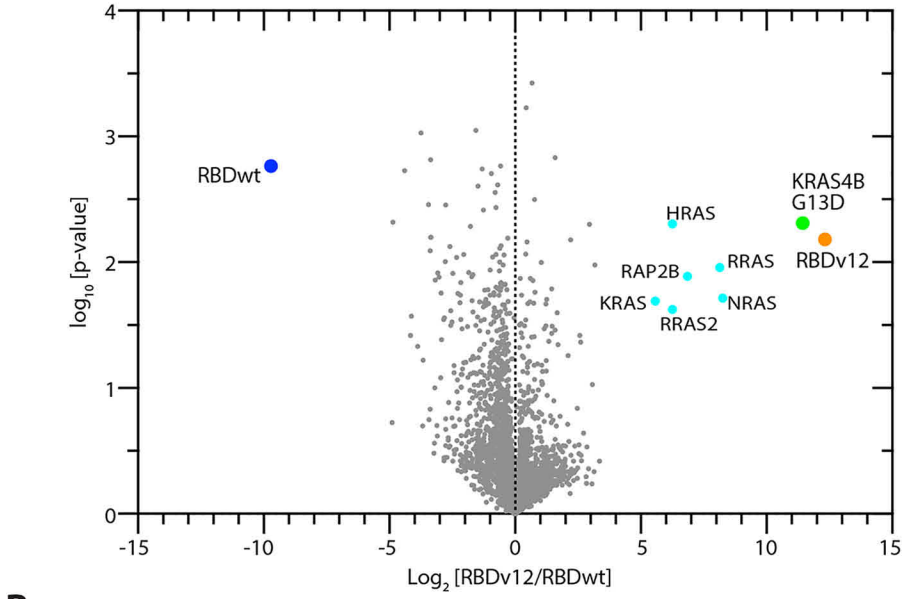

B

Switch 1

```
KRAS   17 SALTIQLIQNHFVDEYDPTIEDSYRKQVVIDGETCLLDILDTAG 60
HRAS   17 ----------------|------|---------------------- 60
NRAS   17 ----------------|------|---------------------- 60
RRAS   43 ------F--SY--SD--------|--T-ICSV--IPAR-------- 86
RRAS2  28 ------F--SY--TD--------|--T--C---DRAAR-------- 71
RAP1A  17 ----V-FV-GI--EK--------|------EV-CQQ-M-E------ 60
RAP1B  17 ----V-FV-GI--EK--------|------EV-AQQ-M-E------ 60
RAP2A  17 ----V-FVTGT-IEK--------|F---EIEV-SSPSV-E------ 60
RAP2B  17 ----V-FVTGS-IEK--------|F---EIEV-SSPSV-E------ 60
RAP2C  17 ----V-FVTGT-IEK--------|F---EIEV-SSPSV-E------ 60
```

Figure 3. RBDvs are specifically binding to endogenous KRAS4B G13D in HCT 116 cells. *A*, mass spectrometry of co-immunoprecipitation using anti-HA beads from lentiviral transduced HCT 116 cells stably expressing HA-tagged RBDwt, RBDv1, and RBDv12 upon induction with doxycycline (DOX) (1 μg/ml, 24 h). Detected proteins (*gray*) were plotted as $\log_2$ average protein intensity for RBDv1/RBDwt (*top*) or RBDv12/RBDwt (*bottom*) *versus* $\log_{10}$ *p* value. More than 16-fold enriched proteins and the RBDvs are shown as indicated (*colored symbols*). *B*, sequence alignment of Ras GTPases that have been enriched more than 16-fold ($\log_2 > 4$). Conserved residues relative to KRAS are indicated as *dashes*. Switch-1 residues (*blue box*) and contact residues within 4.5 Å of RBDvs (*magenta*) are *highlighted*.

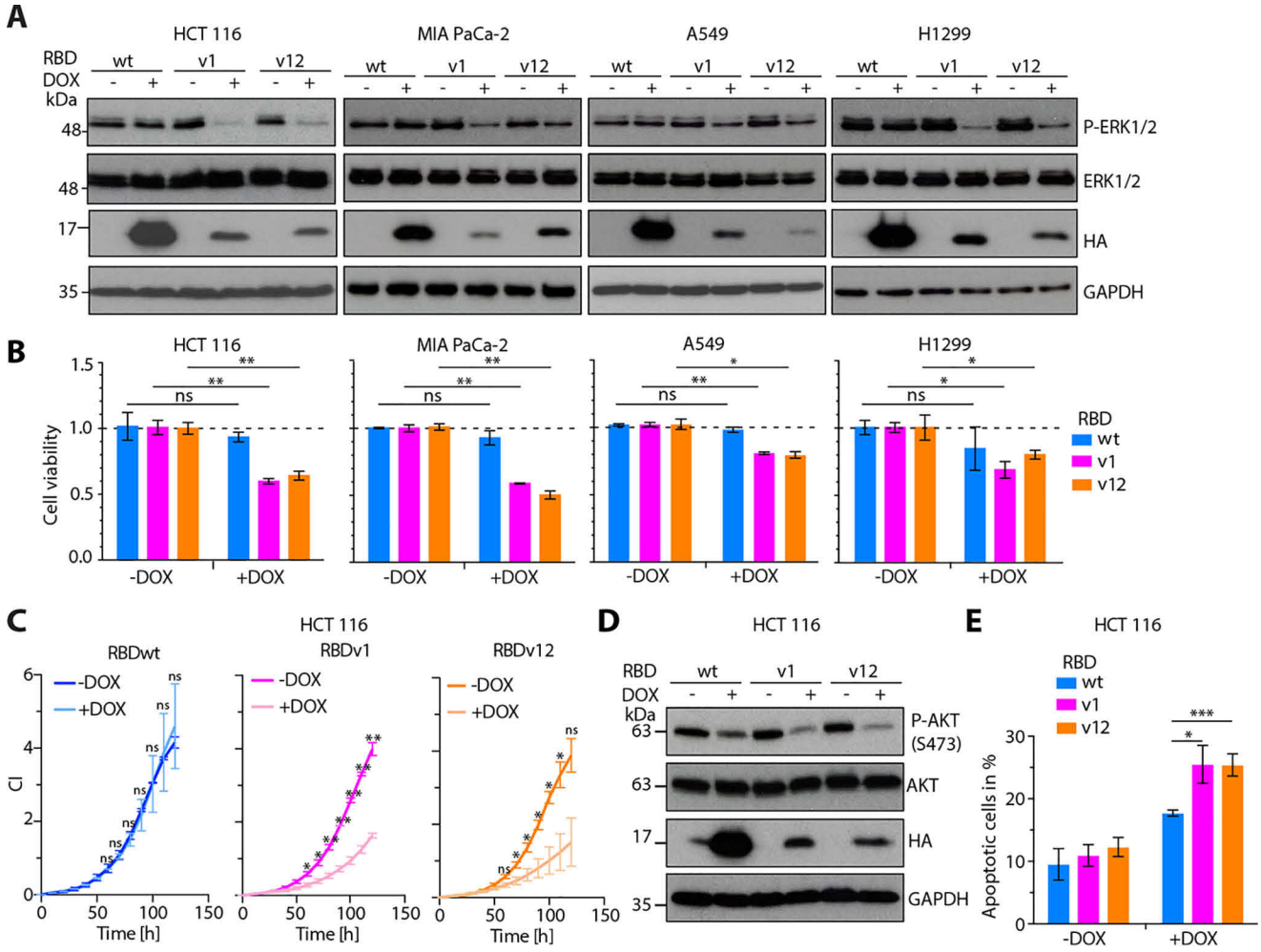

Figure 4. RBDvs inhibit MAPK and PI3K signaling in cancer cells, reduce cellular viability, and induce apoptosis in HCT 116 cells. *A*, immunoblot analysis of whole-cell lysates from HCT 116, MIA PaCa-2, A549, and H1299 stably transduced with inducible lentiviral constructs expressing HA-tagged RBDwt, RBDv1, or RBDv12 in the absence (−) and presence (+) of DOX (1 μg/ml, 24 h). Cell lysates were analyzed using the indicated antibodies. *B*, normalized cell viability from cells used in *A* transduced with RBDwt (*blue*), RBDv1 (*magenta*), or RBDv12 (*orange*) measured as cellular ATP content by luciferase-mediated bioluminescence. Reduction of cellular ATP in the presence of RBDs (+*DOX*) was monitored after 120-h induction and normalized to the luminescence of noninduced control (−*DOX*) cells. *Error bars*, S.D. of three biological replicates ($n = 3$). *C*, cellular growth measured following cell index over time (h) by RTCA of HCT 116 cells in the absence or presence of DOX (1 μg/ml, 120 h). The mean of two technical replicates is shown. *D*, immunoblot analysis of whole-cell lysates from HCT 116 stably transduced with RBDwt, RBDv1, or RBDv12 in the absence (−) and presence (+) of DOX (1 μg/ml, 24 h). Cell lysates were analyzed using the indicated antibodies. *E*, quantification of flow cytometry data of annexin V antibody and propidium iodide–stained HCT 116 cells cultured under full medium conditions in absence (−*DOX*) or presence (+*DOX*) (1 μg/ml, 72 h). *Error bars*, S.D. of three biological replicates ($n = 3$). *p* values were calculated by an unpaired *t* test (*, $p < 0.05$; *, $p < 0.01$; ***, $p < 0.005$; *ns*, not significant).

Table 1

Summary of response to Ras inhibition and mutational status of tested CRC organoids

P, patient; T, tumor; MSI, microsatellite instability; NA, not available.

HUB tumor organoid (29)	Organoid response in the presence of RBDvs				Published mutational status (29)				
	pERK	pAKT	Cell viability	Colony growth	Geftinib sensitivity	KRAS	NRAS	BRAF	PI3K
P6T	↓	–	↓	↓	Resistant	G12C	WT	WT	WT
P26T	–	–	–	–	Resistant	G12V	WT	WT	WT
P28T	↓	↓	↓	↓	Sensitive	G12V	WT	WT	WT
P17T	↓	↓	↓	↓	Sensitive	WT	WT	WT	WT
P18T	–	–	–	–	Resistant	WT	WT	WT	WT
P20T	–	–	–	–	Sensitive	WT	WT	WT	WT
P24bT (MSI)	↓	↓	↓	↓	NA	WT	WT	WT	WT

phorylation (Fig. 5*A*). P18T with WT KRAS showed little effect of either RBDv1 or RBDv12 (Fig. S5*A*). This is consistent with different cancers having diverse adaptive signaling pathways and different signaling dependences.

Despite the variability in the effects on kinase phosphorylation, subsets of the organoids with mutant Ras (P6T and P28T) and those with WT Ras (P17T and P24bT) had reduced viability when expressing either RBDv1 or RBDv12, as indicated by reduced metabolic activity (ATP content) (Fig. 5*B*). In addition, the effect of RBDvs on cell viability correlated with decreased colony size as determined by bright field microscopy (Fig. 5*C*). Importantly, quantification of the colony size indicated that the

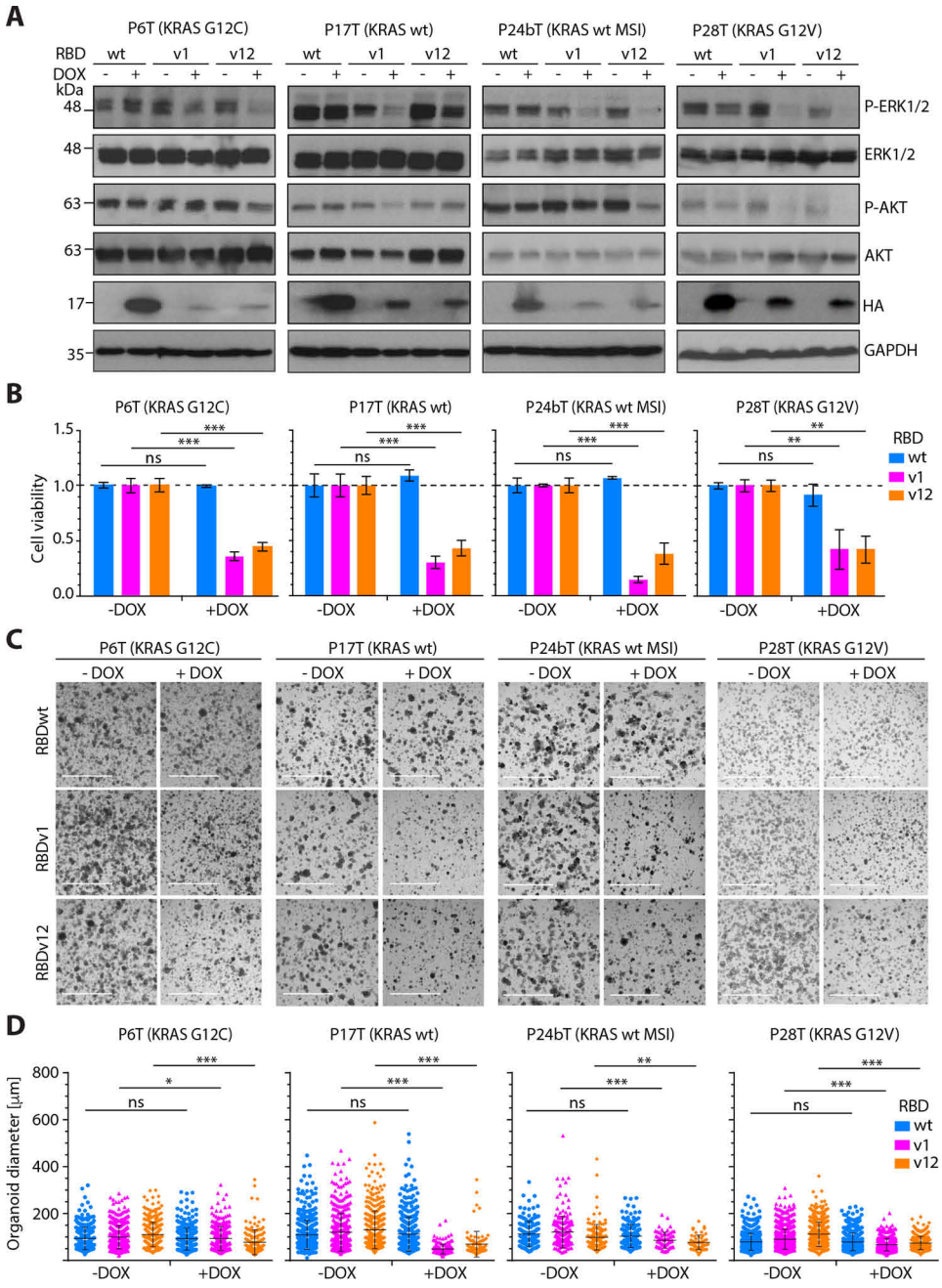

Figure 5. Patient-derived CRC organoids show reduced MAPK and AKT signaling and reduced cell viability upon RBDv expression. *A*, immunoblot analysis of whole-cell lysates derived from the indicated patient-derived CRC organoids stably transduced with lentivirus encoding HA-tagged RBDwt, RBDv1, and RBDv12 in the absence (−) or presence (+) of DOX (2 μg/ml, 72 h). Cell lysates were analyzed using the indicated antibodies. *B*, cellular ATP content of organoid cultures used in *A* expressing RBDwt (*blue*), RBDv1 (*magenta*), and RBDv12 (*orange*) was measured in a luciferase-mediated bioluminescence assay. Reduction of cellular ATP in the presence of RBDvs (+*DOX*) in P17T and P24bT was monitored after a 72-h induction and normalized to the luminescence of noninduced control organoids (−*DOX*) (2 μg/ml, 72 h). P6T and P28T stable organoids were seeded as single cells and induced for 96 h and analyzed as above. *Error bars*, S.D. of three technical replicates ($n = 3$). *C*, bright field microscope images of organoid cultures used in *A* in the presence (+) or absence (−) of DOX (2 μg/ml, 2–6 days). *Scale bars*, 2 mm. *P*, patient; *T*, tumor; *MSI*, microsatellite instability. *D*, quantification of organoid size in the presence and absence of DOX (2 μg/ml, 2–6 days) from bright field microscope images of organoid lines used in *A*. *Error bars*, S.D. Statistics were calculated using an unpaired *t* test in *B*, and the Mann–Whitney *U* test in *D* (*, $p < 0.05$; **, $p < 0.01$; ***, $p < 0.005$; *ns*, not significant).

inhibitory RBDvs significantly reduced growth when compared with noninduced organoids (Fig. 5*D*). However, growth of P18T and P20T, both with WT KRAS, and P26T with KRAS G12V was unaffected by either RBDv1 or RBDv12 (Fig. S5*B*). Thus, KRAS mutant status was insufficient to predict sensitivity to the growth-inhibiting effects of Ras inhibition (Table 1). Our data indicated that the RBDvs classify colorectal cancer samples for Ras dependence. The difference in responsiveness to RBDvs was not related to downstream activation of growth signaling by mutant BRAF, PI3K, or other mutations in the MAPK pathway in these organoids, because we tested organoids that are largely WT for BRAF, PI3K, and other MAPK pathway proteins (29). In conclusion, the RBDvs decreased the growth of four patient-derived organoid lines,

indicating that inhibiting the interactions between activated Ras proteins and their effectors may be a valid strategy in cancer therapy.

Discussion

By engineering the Ras/Raf interface of the CRAF-RBD, we developed potent and highly selective inhibitors of activated Ras that outcompete the binding of signaling effectors. The selectivity of the engineered variants for an active conformation of Ras occurred through molecular contacts to a minimal epitope composed of switch-1 residues at the center of the effector-binding site. High affinity was achieved by a subtle rewiring of the hydrogen-bond pattern at the interface between the RBD and HRAS. Because the effector-binding site is conserved among Ras family members, we detected interactions between the RBDvs and other Ras-subfamily GTPases with nearly identical sequence composition in the switch-1 region. Due to this high degree of sequence conservation within the Ras subfamily, a further optimization of the intermolecular contacts to achieve selectivity to KRAS, HRAS, or NRAS would be very difficult and most likely result in an identical or at least highly similar hydrogen-bonding pattern. Nevertheless, this multispecificity may be beneficial for therapeutic applications based on the RBDvs, because cancer cells often develop resistance to highly specific targeted therapies (30, 31). The ability to inhibit multiple related Ras family members specifically in the active conformation may prevent a bypass or network rewiring that enables resistance, may interfere with other pathways that collectively provide cancer cells a growth advantage, or may sensitize cancer cells to other therapeutics.

In cellular experiments, expression of RBDvs efficiently reduced ERK and AKT phosphorylation and cellular growth and triggered apoptosis in cell lines from different cancer backgrounds. We applied the RBDvs to a clinical research question and showed that the RBDvs could be used as a tool to delineate Ras dependence in colorectal cancer carcinoma (CRC) (29). In CRC, several different signaling pathways have been implicated in disease pathogenesis (32). However, the extent and heterogeneity of genetic alterations in CRC makes it difficult to analyze the contribution of individual pathways to the proliferative phenotype (29). More importantly, this diversity makes defining an effective treatment strategy challenging. We showed that the inhibition observed in adherent cell culture experiments translates to patient-derived colorectal cancer organoids: Several of the organoids exhibited reduced growth when expressing either RBDv1 or RBDv12. However, indicative of their varying degree of Ras dependence, not all organoids responded equally well to Ras inhibition by the inhibitory RBDvs. Unexpectedly, the Ras dependence did not correspond to the presence of mutant Ras, showing that genetic information is insufficient to predict therapeutic response. Thus, the RBDvs can be used to facilitate functional classification of Ras dependence in intestinal tumor organoids, which has the potential to drive therapeutic strategies.

Although the RBDvs are a unique tool for studying Ras-dependent signaling processes, several intracellular affinity reagents targeting GTP-bound Ras have been reported (13, 15–17). Compared with the previously reported Ras-targeted reagents, the RBDvs were effective at lower concentrations. For example, the affinity reagent R11.1.6, based on a DNA-binding domain from a thermophilic archaeon, binds Ras in an active conformation and competes with effector binding (15). Although initial experiments in HEK293T cells suggested otherwise, R11.1.6 does not affect Ras-mediated signaling in a broad range of cancer cell lines (20). Kauke *et al.* (20) concluded that a higher concentration of R11.1.6 than was achieved by lentiviral transduction is required to efficiently outcompete Ras-binding effectors. Similar observations have been made for intracellular antibodies targeting the Ras effector-binding interface. The antibody fragment iDab#6 required the addition of a membrane localization peptide to overcome the binding avidity of endogenous Ras effectors to inhibit Ras-dependent signaling events (16). The cell-penetrating TMab4 RT11 antibody targeting the switch-1 site of Ras proteins also requires high concentrations to effectively inhibit Ras-mediated signaling events (17). Two designed ankyrin repeat proteins (DARPins) with specificity for either the GDP-bound inactive state (K27) or the GTP-bound active state (K55) of Ras have been reported (13). Both DARPins inhibit Ras signaling in transfected HEK293T cells and lentivirus-transduced HCT 116 cells; however, it remains to be seen whether the observed effects occur in other cell types and organoids. The lower affinity of K55 (167 nM) compared with that of CRAF-RBDwt (~60–80 nM) for GTP-bound Ras also suggests that a high concentration will be required to compete for endogenous effectors in a cellular context.

In contrast to these other Ras interaction inhibitors, the intracellular inhibition of Ras signaling by the RBDvs does not show similar avidity or concentration-dependent effects. Indeed, we observed robust inhibition in several different cell lines and organoids despite the fact that the expression of the RBDvs was always less than the corresponding WT control. The RBDvs exhibited preferential binding to active Ras proteins, indicating high selectivity not only for Ras proteins with a shared effector-binding site but also for these proteins in their active conformation. Most likely, the other interaction inhibitors, especially TMab4 RT11 that also binds the switch-1 sequence, may also have similar multispecificity for Ras proteins. This potential property of the other affinity reagents should be further examined.

A common challenge in all of these efforts is the effective delivery of intracellular affinity reagents to the cytosol. Consequently, various intracellular protein delivery platforms, such as cell-penetrating peptides, nanocarrier, liposomes, polymer, and nanoparticle-stabilized nanocapsules (reviewed in Ref. 33), are actively under investigation. Another promising strategy for the delivery of proteins into mammalian cells is the use of bacterial toxins, which can deliver a wide array of passenger proteins spanning a range of sizes, structures, and stabilities (34). For example, a recent report shows that a fusion protein of the RBDwt is able to pass through the channel of a tripartite toxin complex (Tc toxins) derived from bacterial pathogens. Thus, due to its small size and favorable charge distribution, the RBD-scaffold may be particularly suited for delivery by Tc toxins (35). In the future, these and other platforms can enable targeted delivery of proteins into cells to realize the potential of

protein-based therapeutics with intracellular sites of action. RBDvs would then be a candidate for delivery to test in treating diseases associated with unchecked Ras activity.

Experimental procedures

Ras expression, purification, and nucleotide exchange

The human HRAS (AA 1–166) and KRAS (AA 1–169, isoform B) proteins were expressed as GST fusions from pGEX-6P-1 plasmids for selection experiments and as His tag fusions from pET-53 plasmids for *in vitro* competition and binding assays. Plasmids were used to transform *Escherichia coli* Rosetta(DE3) cells, and individual colonies were handled essentially as described (22), except that all buffers were supplemented with 5 mM $MgCl_2$. Briefly, resulting cultures from individual colonies were inoculated into Luria Broth media, and protein expression was induced at A_{600} = 0.8 with 0.5 mM isopropyl 1-thio-β-D-galactopyranoside. After overnight incubation at 16 °C, bacterial pellets were resuspended in 50 mM Tris-HCl, pH 7.5, 150 mM NaCl, 1 mM PMSF, and 5 mM $MgCl_2$ and lysed by sonication. The lysates were clarified by centrifugation, and proteins in the supernatant were purified using nickel-nitrilotriacetic acid chromatography (Qiagen) for His-tagged proteins or GSH Sepharose 4 Fast Flow beads (GE Healthcare) for GST-tagged proteins at 4 °C following the manufacturer's instructions. Eluted fractions were dialyzed into 150 mM NaCl, 50 mM Tris-HCl, pH 7.5, 1 mM DTT, and 5 mM $MgCl_2$, and protein concentrations were determined by measuring the absorption at 280 nm. Nucleotide exchange to GTPγS or GDP was performed by the addition of a 10-fold molar excess of GTPγS or GDP (Sigma–Aldrich) and 5 mM EDTA to dialyzed proteins. After a 30-min incubation at 37 °C, proteins were transferred on ice, and exchange was quenched by the addition of a 10 mM $MgCl_2$ final concentration.

Construction of a phage-displayed CRAF-RBD library

For phage library construction, the RBD of human CRAF kinase (AA 55–131) was cloned into the phagemid pNE (21), and cysteines at positions 81, 95, and 96 of the RBD were mutated to serines using site-directed mutagenesis (36). Afterward, two degenerate oligonucleotides were used to introduce mutations at two regions of the RBD gene by site-directed mutagenesis (21, 22). The nucleotide ratio at the targeted position was adjusted to 70% of the WT nucleotide, represented as N1 = A, N2 = C, N3 = G, and N4 = T, and 10% of each of the other three nucleotides: Oligonucleotide 1, GAT GAC AAA AGC AAC N1N2N4 ATC N2N3N4 GTT N4N4N2 TTG CCG AAC N1N1N3 N2N1N1 N1N3N1 ACA N3N4N3 GTC N1N1N4 GTG CGA AAT GGA ATG; Oligonucleotide 2, CAT GAC TGC CTT ATG N1N1N1 N3N2N1 CTC N1N1N3 N3N4N3 N2N3N3 N3N3N2 CTG CAG CCA GAG TGC. The resulting library was used to electroporate *E. coli* SS320 cells using established methods, resulting in 2.2×10^9 independent RBD variants (37).

RBD variant selection against activated HRAS

A library pool of phage displaying individual RBD variants was harvested by precipitation with PEG/NaCl (20% PEG 8000 (w/v), 2.5 M NaCl) and resuspended in PBT buffer (1× PBS, 1% BSA, 0.1% Tween 20) supplemented with 5 mM $MgCl_2$. Immobilization of GTPγS-loaded GST-tagged HRAS and subsequent binding selections were done essentially as described before (22), except that all buffers were supplemented with 5 mM $MgCl_2$. In brief, four wells of a 96-well Maxisorp microtiter plate (NUNC) were coated with 100 μl of 2 μM GST-tagged GTPγS-loaded HRAS in dialysis buffer (150 mM NaCl, 50 mM Tris-HCl, pH 7.5, 1 mM DTT, and 5 mM $MgCl_2$) overnight at 4 °C. After blocking with PBT buffer for 1 h, the phage library pool was added to each well and incubated for 1 h at 4 °C. The plate was washed eight times with cold PT buffer (1× PBS, 0.1% Tween 20), and bound phage were eluted with 0.1 M HCl and immediately neutralized with 1.0 M Tris-HCl, pH 8.0. Eluted phage were directly used to infect exponentially growing *E. coli* XL1-blue supplemented with helper phage M13K07 (New England Biolabs) and incubated overnight at 37 °C. In each successive selection round, the selection stringency was increased by two additional washing steps, and to avoid unspecific binding toward the GST tag, a GST counterselection was performed starting with round 2. Additionally, after three rounds of selection, phage binding and washing was done at room temperature, and the concentration of coated GST-tagged GTPγS-loaded HRAS was reduced to 0.5 μM. After five rounds of enrichment, individual RBD variants with improved binding properties toward active HRAS were identified by clonal phage ELISA as described (37). In brief, phage displaying individual RBD variants were prepared from single colonies of bacteria harboring phagemids encoding RBDvs and transferred to 384-well Maxisorp plates immobilized with GST-tagged GTPγS-labeled HRAS (0.5 μM) and blocked with BSA, as described previously. As negative controls, wells were coated with GST or only blocked with BSA. After incubation, washing, and developing, positive clones were further analyzed by sequencing.

Cloning of RBD variants

DNA fragments encoding the selected variants and the unmodified RBDwt were cloned into pDONR233 plasmids by Gateway cloning (Invitrogen) as described (22). Further recombination into the Gateway destination vectors pET53DEST, pDEST15, and pLDT-NT-HA was performed according to the manufacturer's instructions (Invitrogen).

RBDvs protein expression and purification

For competitive *in vitro* pulldown experiments and bio-layer interferometry measurements, His-tagged (from pET53DEST plasmids) and GST-tagged (from pGEX-6p-1 plasmids) RBD variants and RBDwt, Ras-association domain (RA) of RalGDS (AA 798 – 885) and GST alone were processed as Ras proteins (see above).

Competitive in vitro pulldown experiment

The Ras/RBDwt competition assay was performed in 200 μl of assay buffer (25 mM Tris-HCl, pH 7.5, 150 mM NaCl, 1% Nonidet P-40, 5 mM $MgCl_2$, and 5% glycerol) using 8 μg (1.15 μM) of GST-tagged RBDwt or RalGDS-RA bound to GSH-Sepharose beads. First, 5 μg (1.15 μM) of His-tagged KRAS loaded with GTPγS was incubated with His-tagged RBDwt or RBDvs

with increasing concentrations (2.3 μg (1.15 μM), 5.8 μg (2.68 μM), and 23 μg (11.5 μM), which corresponds to a molar ratio of 1:1, 1:2.5, and 1:10 of GST-tagged RBDwt or RalGDS-RA:His-tagged RBDwt or RBDvs) for 30 min at 4 °C with end-over-end rotation. Eight μg of beads were added to the reaction mix and incubated for another 30 min at 4 °C. After two washes with assay buffer, beads were resuspended in 30 μl of 2× SDS sample buffer and incubated for 5 min at 95 °C. Control samples consisted of GTPγS- or GDP-loaded KRAS incubated with GST-RBDwt or GST-RalGDS-RA beads. Also, GTPγS-loaded KRAS was incubated with GST bound to beads. Samples were analyzed by immunoblot analysis using anti-Ras antibody (catalog no. 16117, Thermo Fisher Scientific), and membrane was stained with Ponceau S as loading control.

Bio-layer interferometry

Kinetic binding assays were performed on an Octet RED96 instrument (Pall ForteBio). Dialyzed proteins were supplemented with 0.1% BSA and 0.02% Tween 20. GST-tagged RBDvs were immobilized onto anti-GST biosensors (Pall ForteBio) at a concentration of 2 μg/ml. Association was analyzed at concentrations starting from 1000 to 15.6 nM in 1:1 dilution steps of GTPγS- or GDP-loaded HRAS. Dissociation was measured in dialysis buffer (150 mM NaCl, 50 mM Tris-HCl, pH 7.5, 1 mM DTT, and 5 mM $MgCl_2$) supplemented with 0.1% BSA and 0.02% Tween 20. Nonspecific interaction of HRAS with biosensors or GST was assayed using empty anti-GST sensors or GST immobilized on anti-GST sensors (2 μg/ml). Reference wells were subtracted from sample wells, and a 1:1 global fitting model was used to determine k_{on}, k_{off}, and K_d values.

Protein expression and purification for crystallography

RBDv1, RBDv12, and HRAS G12V (residues 1–166) were expressed as TEV protease–cleavable GST fusions using a modified pGEX-2T vector. Expression constructs were transformed into BL21-CodonPlus DE3-RIL bacteria (Agilent Technologies) for protein production. Bacterial expression was induced overnight at 18 °C with 0.5 mM isopropyl 1-thio-β-D-galactopyranoside and was performed in Luria broth media. RBDvs bacterial pellets were resuspended in 50 mM HEPES, pH 7.5, 300 mM NaCl, 5% glycerol, 1 mM PMSF, 1 mM TCEP and lysed by homogenization. The lysate was cleared by centrifugation at 4 °C for 40 min at 18,000 × *g*. Protein was bound to GSH affinity resin (GE Healthcare), eluted by cleavage of the GST tag with TEV, concentrated, and then buffer-exchanged by size-exclusion chromatography (SEC) using a Superdex75 24-ml column (GE Healthcare) equilibrated in 50 mM HEPES, pH 7.5, 50 mM NaCl, 5% glycerol, 10 mM $MgCl_2$, 1 mM TCEP.

HRAS G12V bacterial pellets were resuspended in 50 mM HEPES, pH 7.5, 300 mM NaCl, 5 mM EDTA, 5% glycerol, 1 mM PMSF, 1 mM TCEP and lysed by homogenization. The lysate was clarified by centrifugation at 4 °C for 40 min at 18,000 × *g*. Protein was bound to GSH affinity resin (GE Healthcare), washed with 50 mM HEPES, pH 7.5, 300 mM NaCl, 25 mM imidazole, 5% glycerol, 1 mM TCEP and eluted by cleavage of the GST tag with TEV. After concentrating, the buffer was exchanged by SEC using a Superdex75 24 ml column equilibrated in 50 mM HEPES pH 7.5, 300 mM NaCl, 5 mM EDTA, 5% glycerol, 1 mM TCEP. GMP-PNP loading on HRAS G12V was carried out by incubating purified HRAS G12V with a 10-fold excess of GMP-PNP for 80 min at 4 °C, followed by the addition of a 30-fold excess of $MgCl_2$ for 120 min at 4 °C.

The RBDvs:HRAS G12V complexes were obtained by mixing RBDvs and GMP-PNP–loaded HRAS G12V at equal molar ratios for 60 min at 4 °C, followed by SEC using a Superdex75 24-ml column equilibrated in 50 mM HEPES, pH 7.5, 50 mM NaCl, 10 mM $MgCl_2$, 5% glycerol, 1 mM TCEP. All fractions corresponding to co-elution of HRAS G12V with RBDvs were pooled and concentrated to 12.2 mg/ml and then flash-frozen in liquid nitrogen. Protein concentration was estimated by UV-visible absorption spectroscopy using a NanoDrop spectrophotometer (Thermo Fisher Scientific).

Protein crystallography, data collection, and structural analysis

The RBDvs:HRAS G12V complexes were crystallized at 20 °C in sitting-drop by mixing 0.5 μl of complexes (450 μM, 12.2 mg/ml) with 0.5 μl of mother liquor of 0.1 M sodium cacodylate, pH 6.5, 200 mM ammonium sulfate, 30% PEG 4000, or mother liquor of 0.1 M sodium citrate, pH 5.6, 200 mM ammonium sulfate, 30% PEG 4000 for RBDv1:HRAS G12V and RBDv12:HRAS G12V, respectively. X-ray diffraction data were collected on a flash-frozen crystal cryoprotected in mother liquor containing 25% glycerol at 100 K on station 24-ID-C, NE-CAT beamline, Advanced Photon Source. Data reduction was performed using the XDS package (38). The structure was solved by molecular replacement using PDB entry 4G0N (5) as a search model in Phaser (39). Model building and refinement were performed using COOT (40), LORESTR (41), and REFMAC (42) from the CCP4 suite (43) and Phenix (44). The data statistics and refinement details are reported in Table S1. The distance of hydrogen bonds and salt bridges was measured using the PDBeISA interactive tool (RRID:SCR_015749) (45). The difference of the center of mass positions and rotation angles of the RBD variants was calculated using the PyMOL script: draw_rotatio_axis (RRID:SCR_018124).

Alanine scanning

Alanine mutations of RBDv12 at positions Leu^{61}, His^{65}, Glu^{66}, Lys^{71}, Arg^{88}, and His^{89} were introduced using site-directed mutagenesis (36). Phage displaying RBDv12 and RBDv12 alanine mutants were prepared from single colonies of bacteria transformed with phagemids encoding RBDv12 and RBDv12 alanine mutants using established methods (37). Binding to active HRAS was tested by phage ELISA. In short, the phage solution was transferred to immobilized GTPγS-loaded GST-tagged HRAS (1 μM in 1× PBS) and anti-FLAG-M2 control (diluted 1:5000 in 1× PBS, Sigma–Aldrich) in a 96-well Maxisorp microtiter plate (NUNC) and incubated for 60 min at room temperature. After washing with PT buffer, bound phage were detected by the addition of anti-M13 antibody (GE Healthcare) fused to horseradish peroxidase and developed with TMB substrate (BD Biosciences).

Cell culture

HCT 116 (catalog no. CCL-247) cells were purchased from ATCC and handled according to the supplier's instructions. MIA PaCa-2, A549, and H1299 cell lines were cultured in DMEM (MIA PaCa-2 and A549) or RPMI 1640 (H1299) medium (both from Gibco) supplemented with 10% (v/v) fetal bovine serum (Gibco). Cell lines were tested and found to be mycoplasma-free. Lentiviral particles were produced in HEK293T cells using established protocols (Addgene). Stable cell lines were constructed using lentiviral vectors (pLDT) encoding N-terminally HA-tagged RBDvs and WT under the control of a doxycycline-inducible promotor by standard techniques (47). The original pLDT plasmid was a gift from Jason Moffat (University of Toronto). Two days after transduction, cell lines were selected with 2 μg/ml puromycin for HCT 116, MIA PaCa-2, A549, and H1299. For all experiments, 1 μg/ml doxycycline was used to induce expression of HA-tagged RBDvs or RBDwt.

Immunoprecipitation for MS

Two 10-cm dishes per construct (RBDwt, RBDv1, and RBDv12) were seeded with 2 $\times$ 10^6/ml stable HCT 116 cells, and RBDv expression was induced 24 h later with doxycycline. After a 24-h induction, cells were scraped into 1$\times$ PBS and washed twice with 1$\times$ PBS. After centrifugation, the cell pellets were resuspended in lysis buffer (25 mM Tris-HCl, pH 7.5, 150 mM NaCl, 1% Nonidet P-40, 5 mM $MgCl_2$, 5% glycerol, and protease inhibitor mixture (Roche Applied Science)) and incubated for 20 min at 4 °C with end-over-end rotation. The lysates were centrifuged, and supernatants were transferred to 20 μl of pre-equilibrated anti-HA affinity matrix (Roche Applied Science) and incubated for 40 min at 4 °C. Beads were washed two times with 500 μl of lysis buffer. Elution was performed by the addition of 20 μl of 2$\times$ SDS-sample buffer to the beads and incubation for 3 min at 95 °C. 5 μl of samples were analyzed by immunoblotting using antibodies against endogenous Ras, HA tag, and GAPDH (catalog nos. 3965, 2999, and 8884, respectively; all from Cell Signaling Technology). Sample preparation for in-gel digest was done as described before (48). In brief, supernatants were loaded onto SDS-polyacrylamide gel, and the gel was stained using InstantBlue (Expedeon). Gel lanes were cut into pieces and subsequently washed, destained, and dehydrated. Proteins were reduced with 10 mM DTT, alkylated with 55 mM iodoacetamide, and digested overnight with sequencing-grade trypsin (Promega). Peptides were extracted using an increasing concentration of acetonitrile. Finally, peptides were concentrated and desalted using the Stop and Go Extraction (STAGE) technique (49).

Liquid chromatography and MS

A binary buffer system consisting of buffer A (0.1% formic acid) and buffer B (80% acetonitrile, 0.1% formic acid) was used for peptide separation on an Easy-nLC 1200 (Thermo Fisher Scientific). This system was coupled via a nano-electrospray ionization source to the quadrupole-based Q Exactive HF benchtop mass spectrometer (50). Peptide elution from the in-house packed 18-cm (1.9-μm C18 Beads, Dr. Maisch HPLC GmbH, Ammerbuch, Germany) column was achieved by increasing the relative amount of B from 10 to 38% in a linear gradient within 23 min at a column temperature of 40 °C. Followed by an increase to 100% B within 7 min, gradients were completed by a re-equilibration to 5% B.

Q Exactive HF settings

MS spectra were acquired using 3E6 as an AGC target, a maximal injection time of 20 ms, and a 60,000 resolution at 300 m/z. The mass spectrometer operated in a data-dependent Top15 mode with subsequent acquisition of higher-energy collisional dissociation (HCD) fragmentation MS/MS spectra of the top 15 most intense peaks. Resolution for MS/MS spectra was set to 30,000 at 200 m/z, AGC target to 1E5, maximal injection time to 64 ms, and the isolation window to 1.6 Thomson.

Mass spectrometry data processing and analysis

All acquired raw files were processed using MaxQuant (version 1.5.3.30) (51) and the implemented Andromeda search engine (52). For protein assignment, electrospray ionization-tandem MS fragmentation spectra were correlated with the Uniprot human database (version 2016), including four manually added sequences of the RBD variants and KRAS G13D (RBDwt, MGYPYDVPDYAGQGPDPSTNSADITSLYKKAGF-SNTIRVFLPNKQRTVVNVRNGMSLHDCLMKALKVRGLQ-PECCAVFRLLHEHKGKKARLDWNTDAASLIGEELQVDFL; RBDv1, MGYPYDVPDYAGQGPDPSTNSADITSLYKKAGF-SNTIRVLLPNQEWTVVKVRNGMSLHDSLMKALKRHGLQ-PESSAVFRLLHEHKGKKARLDWNTDAASLIGEELQVDFL; RBDv12, MGYPYDVPDYAGQGPDPSTNSADITSLYKKAG-FSNTIRVLLPNHERTVVKVRNGMSLHDSLMKALKRHGLQ-PESSAVFRLLHEHKGKKARLDWNTDAASLIGEELQVDFL; KRAS G13D, MTEYKLVVVGAGDVGKSALTIQLIQNHFV-DEYDPTIEDSYRKQVVIDGETCLLDILDTAGQEEYSAMRD-QYMRTGEGFLCVFAINNTKSFEDIHHYREQIKRVKDSED-VPMVLVGNKCDLPSRTVDTKQAQDLARSYGIPFIETSAK-TRQGVDDAFYTLVREIRKHKEKMSKDGKKKKKKSKTKC-VIM).

The total number of entries of the database searched was 92,169. Searches were performed with tryptic specifications (maximum missed cleavages = 2) and default settings for mass tolerances for MS and MS/MS spectra (20 ppm for first search, 4.5 ppm for main search (precursor mass tolerance), and 20 ppm fragment mass tolerance). Carbamidomethyl at cysteine residues was set as a fixed modification, whereas oxidation at methionine and acetylation at the N terminus were defined as variable modifications. The minimal peptide length was set to seven amino acids, and the false discovery rate for proteins and peptide-spectrum matches was set to 1%. The match-between-run feature was used with a time window of 0.7 min. Relative label-free quantification of proteins was done using the MaxLFQ algorithm integrated into MaxQuant (53). The minimum LFQ ratio count was set to 2, and the FastLFQ option was enabled.

For subsequent analysis, the Perseus software (version 1.5.3.0) (54) was used and first filtered for contaminants and reverse entries and proteins that were only identified by site. The LFQ intensities were logarithmized to base 2 and grouped into duplicates. To overcome the missing value problem in

immunoprecipitation data, proteins that were quantified less than two times in one of the experimental groups were discarded from further analysis. Missing values were imputed column-wise by a down-shifted (median − 1.8) Gaussian distribution mimicking the detection limit of the mass spectrometer.

Metabolic activity assay

1000 cells of each stable cell line were seeded in a 96-well plate in duplicates. The following day, expression was induced by the addition of doxycycline. Corresponding control wells were not induced. Cell viability was assayed 120 h after induction using CellTiter-Glo (Promega). Luminescence signals of induced wells were normalized to uninduced well data.

Immunoblotting

Stable cell lines were seeded in 6-well plates (1×10^5 cells/well) and induced 24 h later with doxycycline (1 μg/ml). Control cells were left uninduced. 24 h after induction, cells were washed twice with 1× PBS and lysed in 200 μl of 2× SDS sample buffer. Whole-cell lysates were analyzed by immunoblotting using the indicated antibodies. For serum starvation experiments, medium was replaced upon induction with serum-free medium. 24 h after induction, cells were treated with 100 ng/ml EGF (Sigma) for 10 min before lysis.

Antibodies

Antibodies used for Western blot analysis were as follows: phospho-ERK1/2 (p44/42 MAPK) (Thr^{202}/Tyr^{204}) (clone D13.14.4E, catalog no. 4370), ERK1/2 (p44/42 MAPK) (clone 137F5, catalog no. 4695), phospho-AKT (Ser^{473}) (clone D9E, catalog no. 4060), AKT (clone C67E7, catalog no. 4691), GAPDH-HRP (clone D16H11, catalog no. 8884), and HA-HRP (clone 6E2, catalog no. 2999). All antibodies were purchased from Cell Signaling Technologies.

Analysis of cell growth by real-time cell analysis (RTCA)

Cell proliferation of stably transduced HCT 116 cells was assessed using the xCELLigence RTCA SP (single-plate) system (ACEA Biosciences). 1000 cells/well were seeded in a 96-well electronic microtiter plate (ACEA Biosciences) with 200 μl of medium/well. After 24 h, cells were induced by doxycycline. Cell proliferation was monitored for 120 h. Experiments were performed as duplicates and repeated at least twice.

Apoptosis analysis by flow cytometry

Stably transduced HCT 116 cells were seeded in 6-well plates (1×10^5 cells/well) and induced 24 h later with doxycycline. Control cells were left uninduced. After 72 h, cells were washed once with 1× PBS. For analysis of apoptotic cells, the annexin V-FITC apoptosis detection kit (catalog no. ALX-850-020 Enzo) was used following the manufacturer's protocol. Samples were analyzed on a FACSCanto II flow cytometer (BD Biosciences), and data were processed by FlowJo software (FlowJo, LLC). Gating was done based on viable and single cells that were identified on the basis of scatter morphology.

Organoid cultures

Human tumor colon organoid samples were obtained from a published colorectal cancer organoid biobank (29). Resection tissues were obtained with written informed consent and following approval by the ethics committees of the Diakonessen Hospital, Utrecht. Tissue was obtained with written informed consent and following approval, according to the guidelines of the University Cancer Center (UCT), Frankfurt. Organoid cultures were established and maintained as described previously (55). Tumor organoids were maintained in medium lacking Wnt3a. The organoid lines were transduced as described (56) with lentivirus expressing N-terminally HA-tagged RBDwt, RBDv1, or RBDv12 (as above). Three days after transduction, organoids were selected with 1 μg/ml puromycin in the culture medium. For cell viability assays, the cells were seeded in Matrigel following either mechanical dissociation or enzymatic single-cell dispersal using TrypLE Express reagent (Gibco). Two μg/ml doxycycline was added 1 day after seeding. After 3 days, cell viability was measured using CellTiter-Glo reagent (Promega). All experiments were measured as technical triplicates, and the experiments were repeated at least twice each.

For quantification of organoid size, light microscopy pictures were taken at a 2× resolution after 2–6 days of doxycycline exposure, as indicated. The diameter (μm) of all viable organoids in one picture of each condition was measured using ImageJ. Viable organoids were identified as refringent, whereas dark structures surrounded by cell debris were excluded from the analysis. The quantification was performed on two independent experiments.

Statistical methods

Data are presented as the mean ± S.D. The comparisons between RBDwt and RBDvs were made by an unpaired *t* test using GraphPad Prism software. For statistical analysis of the quantification results of organoid sizes, a Mann–Whitney *U* test was performed using GraphPad Prism software. The level of significance was set as follows: *, $p < 0.05$; **, $p < 0.01$; ***, $p < 0.005$.

Data and material availability

The atomic coordinates and experimental data of G12V HRAS-GppNHp in complex with RBDv1 (6NTC) and G12V HRAS-GppNHp in complex with RBDv12 (6NTD) have been deposited in the Protein Data Bank. Plasmids used for intracellular expression of HA-tagged RBDwt, RBDv1, or RBDv12 are available on Addgene. The mass spectrometry proteomics data have been deposited to the ProteomeXchange Consortium via the PRIDE (46) partner repository with the data set identifier PXD016827. All data are available in the main text or the supporting materials. All data and material will be made available upon request.

Author contributions—S. W., K. R., and A. E. conceptualization; S. W., B. M. G., M. H., M. K., H. C., I. K., H. F. F., F. S., and A. E. data curation; S. W., P. M., B. M. G., H. C., K. R., H. F. F., F. S., and A. E. validation; S. W., P. M., B. M. G., and A. E. investigation; S. W., P. M., and A. E. visualization; S. W. and A. E. methodology; S. W. and A. E. writing-original draft; S. W., K. R., H. F. F., F. S., and A. E. writing-review and editing; S. W., P. M., B. M. G., M. H., M. K., H. F. F., and A. E. formal analysis; H. C. and K. R. resources; H. F. F., F. S., and A. E. supervision; A. E. funding acquisition; A. E. project administration.

Acknowledgments—We thank Mani Ravichandran from the Structural and Genomic Consortium (SGC) of Toronto for providing X-ray crystallography screening kits. Diffraction work conducted at the Northeastern Collaborative Access Team beamlines was funded by NIGMS, National Institutes of Health (NIH), Grant P41 GM103403 and by NIH-ORIP HEI Grant S10 RR029205. We thank Nancy R. Gough (BioSerendipity, LLC) for constructive comments and editorial assistance. We thank Jason Moffat (University of Toronto) for donation of inducible lentiviral plasmids. We thank Georg Tascher for help in analyzing MS data, Mateusz Putyrski for cloning lentiviral gateway constructs, and Suchithra Guntur and Andrew Vorobyov for assistance during the revision.

References

1. Weber, C. K., Slupsky, J. R., Kalmes, H. A., and Rapp, U. R. (2001) Active Ras induces heterodimerization of cRaf and BRaf. *Cancer Res.* **61,** 3595–3598 Medline
2. Vossler, M. R., Yao, H., York, R. D., Pan, M. G., Rim, C. S., and Stork, P. J. (1997) cAMP activates MAP kinase and Elk-1 through a B-Raf- and Rap1-dependent pathway. *Cell* **89,** 73–82 CrossRef Medline
3. York, R. D., Yao, H., Dillon, T., Ellig, C. L., Eckert, S. P., McCleskey, E. W., and Stork, P. J. (1998) Rap1 mediates sustained MAP kinase activation induced by nerve growth factor. *Nature* **392,** 622–626 CrossRef Medline
4. Yuryev, A., Ono, M., Goff, S. A., Macaluso, F., and Wennogle, L. P. (2000) Isoform-specific localization of A-RAF in mitochondria. *Mol. Cell Biol.* **20,** 4870–4878 CrossRef Medline
5. Fetics, S. K., Guterres, H., Kearney, B. M., Buhrman, G., Ma, B., Nussinov, R., and Mattos, C. (2015) Allosteric effects of the oncogenic RasQ61L mutant on Raf-RBD. *Structure* **23,** 505–516 CrossRef Medline
6. Nassar, N., Horn, G., Herrmann, C., Scherer, A., McCormick, F., and Wittinghofer, A. (1995) The 2.2 Å crystal structure of the Ras-binding domain of the serine/threonine kinase c-Raf1 in complex with Rap1A and a GTP analogue. *Nature* **375,** 554–560 CrossRef Medline
7. Nakhaeizadeh, H., Amin, E., Nakhaei-Rad, S., Dvorsky, R., and Ahmadian, M. R. (2016) The RAS-effector interface: isoform-specific differences in the effector binding regions. *PLoS ONE* **11,** e0167145 CrossRef Medline
8. John, J., Sohmen, R., Feuerstein, J., Linke, R., Wittinghofer, A., and Goody, R. S. (1990) Kinetics of interaction of nucleotides with nucleotide-free H-ras p21. *Biochemistry* **29,** 6058–6065 CrossRef Medline
9. Rudolph, M. G., Linnemann, T., Grunewald, P., Wittinghofer, A., Vetter, I. R., and Herrmann, C. (2001) Thermodynamics of Ras/effector and Cdc42/effector interactions probed by isothermal titration calorimetry. *J. Biol. Chem.* **276,** 23914–23921 CrossRef Medline
10. Cox, A. D., Fesik, S. W., Kimmelman, A. C., Luo, J., and Der, C. J. (2014) Drugging the undruggable RAS: mission possible? *Nat. Rev. Drug Discov.* **13,** 828–851 CrossRef Medline
11. Spencer-Smith, R., Koide, A., Zhou, Y., Eguchi, R. R., Sha, F., Gajwani, P., Santana, D., Gupta, A., Jacobs, M., Herrero-Garcia, E., Cobbert, J., Lavoie, H., Smith, M., Rajakulendran, T., Dowdell, E., Okur, M. N., Dementieva, I., Sicheri, F., Therrien, M., Hancock, J. F., Ikura, M., Koide, S., and O'Bryan, J. P. (2017) Inhibition of RAS function through targeting an allosteric regulatory site. *Nat. Chem. Biol.* **13,** 62–68 CrossRef Medline
12. Khan, I., Spencer-Smith, R., and O'Bryan, J. P. (2019) Targeting the α4-α5 dimerization interface of K-RAS inhibits tumor formation *in vivo*. *Oncogene* **38,** 2984–2993 CrossRef Medline
13. Guillard, S., Kolasinska-Zwierz, P., Debreczeni, J., Breed, J., Zhang, J., Bery, N., Marwood, R., Tart, J., Overman, R., Stocki, P., Mistry, B., Phillips, C., Rabbitts, T., Jackson, R., and Minter, R. (2017) Structural and functional characterization of a DARPin which inhibits Ras nucleotide exchange. *Nat. Commun.* **8,** 16111 CrossRef Medline
14. McGee, J. H., Shim, S. Y., Lee, S. J., Swanson, P. K., Jiang, S. Y., Durney, M. A., and Verdine, G. L. (2018) Exceptionally high-affinity Ras binders that remodel its effector domain. *J. Biol. Chem.* **293,** 3265–3280 CrossRef Medline
15. Kauke, M. J., Traxlmayr, M. W., Parker, J. A., Kiefer, J. D., Knihtila, R., McGee, J., Verdine, G., Mattos, C., and Wittrup, K. D. (2017) An engineered protein antagonist of K-Ras/B-Raf interaction. *Sci. Rep.* **7,** 5831 CrossRef Medline
16. Tanaka, T., Williams, R. L., and Rabbitts, T. H. (2007) Tumour prevention by a single antibody domain targeting the interaction of signal transduction proteins with RAS. *EMBO J.* **26,** 3250–3259 CrossRef Medline
17. Shin, S. M., Choi, D. K., Jung, K., Bae, J., Kim, J. S., Park, S. W., Song, K. H., and Kim, Y. S. (2017) Antibody targeting intracellular oncogenic Ras mutants exerts anti-tumour effects after systemic administration. *Nat. Commun.* **8,** 15090 CrossRef Medline
18. Filchtinski, D., Sharabi, O., Rüppel, A., Vetter, I. R., Herrmann, C., and Shifman, J. M. (2010) What makes Ras an efficient molecular switch: a computational, biophysical, and structural study of Ras-GDP interactions with mutants of Raf. *J. Mol. Biol.* **399,** 422–435 CrossRef Medline
19. Trinh, T. B., Upadhyaya, P., Qian, Z., and Pei, D. (2016) Discovery of a direct Ras inhibitor by screening a combinatorial library of cell-permeable bicyclic peptides. *ACS Comb. Sci.* **18,** 75–85 CrossRef Medline
20. Kauke, M. J., Tisdale, A. W., Kelly, R. L., Braun, C. J., Hemann, M. T., and Wittrup, K. D. (2018) A Raf-competitive K-Ras binder can fail to functionally antagonize signaling. *Mol. Cancer Ther.* **17,** 1773–1780 CrossRef Medline
21. Ernst, A., Avvakumov, G., Tong, J., Fan, Y., Zhao, Y., Alberts, P., Persaud, A., Walker, J. R., Neculai, A. M., Neculai, D., Vorobyov, A., Garg, P., Beatty, L., Chan, P. K., Juang, Y. C., *et al.* (2013) A strategy for modulation of enzymes in the ubiquitin system. *Science* **339,** 590–595 CrossRef Medline
22. Wiechmann, S., Gärtner, A., Kniss, A., Stengl, A., Behrends, C., Rogov, V. V., Rodriguez, M. S., Dötsch, V., Müller, S., and Ernst, A. (2017) Site-specific inhibition of the small ubiquitin-like modifier (SUMO)-conjugating enzyme Ubc9 selectively impairs SUMO chain formation. *J. Biol. Chem.* **292,** 15340–15351 CrossRef Medline
23. Campbell-Valois, F. X., Tarassov, K., and Michnick, S. W. (2005) Massive sequence perturbation of a small protein. *Proc. Natl. Acad. Sci. U.S.A.* **102,** 14988–14993 CrossRef Medline
24. Kiel, C., Filchtinski, D., Spoerner, M., Schreiber, G., Kalbitzer, H. R., and Herrmann, C. (2009) Improved binding of raf to Ras.GDP is correlated with biological activity. *J. Biol. Chem.* **284,** 31893–31902 CrossRef Medline
25. Erijman, A., and Shifman, J. M. (2016) RAS/effector interactions from structural and biophysical perspective. *Mini Rev. Med. Chem.* **16,** 370–375 CrossRef Medline
26. Kiel, C., Serrano, L., and Herrmann, C. (2004) A detailed thermodynamic analysis of ras/effector complex interfaces. *J. Mol. Biol.* **340,** 1039–1058 CrossRef Medline
27. Fridman, M., Maruta, H., Gonez, J., Walker, F., Treutlein, H., Zeng, J., and Burgess, A. (2000) Point mutants of c-raf-1 RBD with elevated binding to v-Ha-Ras. *J. Biol. Chem.* **275,** 30363–30371 CrossRef Medline
28. Burgess, M. R., Hwang, E., Mroue, R., Bielski, C. M., Wandler, A. M., Huang, B. J., Firestone, A. J., Young, A., Lacap, J. A., Crocker, L., Asthana, S., Davis, E. M., Xu, J., Akagi, K., Le Beau, M. M., *et al.* (2017) KRAS allelic imbalance enhances fitness and modulates MAP kinase dependence in cancer. *Cell* **168,** 817–829.e15 CrossRef Medline
29. van de Wetering, M., Francies, H. E., Francis, J. M., Bounova, G., Iorio, F., Pronk, A., van Houdt, W., van Gorp, J., Taylor-Weiner, A., Kester, L., McLaren-Douglas, A., Blokker, J., Jaksani, S., Bartfeld, S., Volckman, R., *et al.* (2015) Prospective derivation of a living organoid biobank of colorectal cancer patients. *Cell* **161,** 933–945 CrossRef Medline
30. Karimkhani, C., Gonzalez, R., and Dellavalle, R. P. (2014) A review of novel therapies for melanoma. *Am. J. Clin. Dermatol.* **15,** 323–337 CrossRef Medline
31. Manzano, J. L., Layos, L., Bugés, C., de Los Llanos Gil, M., Vila, L., Martínez-Balibrea, E., and Martínez-Cardus, A. (2016) Resistant mechanisms to BRAF inhibitors in melanoma. *Ann. Transl. Med.* **4,** 237 CrossRef Medline
32. Fearon, E. R. (2011) Molecular genetics of colorectal cancer. *Annu. Rev. Pathol.* **6,** 479–507 CrossRef Medline

33. Fu, A., Tang, R., Hardie, J., Farkas, M. E., and Rotello, V. M. (2014) Promises and pitfalls of intracellular delivery of proteins. *Bioconjug. Chem.* **25,** 1602–1608 CrossRef Medline
34. Auger, A., Park, M., Nitschke, F., Minassian, L. M., Beilhartz, G. L., Minassian, B. A., and Melnyk, R. A. (2015) Efficient delivery of structurally diverse protein cargo into mammalian cells by a bacterial toxin. *Mol. Pharm.* **12,** 2962–2971 CrossRef Medline
35. Roderer, D., Schubert, E., Sitsel, O., and Raunser, S. (2019) Towards the application of Tc toxins as a universal protein translocation system. *bioRxiv* CrossRef
36. Kunkel, T. A. (1985) Rapid and efficient site-specific mutagenesis without phenotypic selection. *Proc. Natl. Acad. Sci. U.S.A.* **82,** 488–492 CrossRef Medline
37. Fellouse, F. A., and Sidhu, S. S. (2007) Making antibodies in bacteria. in *Making and Using Antibodies* (Howard, G. C., and Kaser, M. R., eds) pp. 157–180, CRC Press, Inc., Boca Raton, FL
38. Kabsch, W. (2010) XDS. *Acta Crystallogr. D Biol. Crystallogr.* **66,** 125–132 CrossRef Medline
39. McCoy, A. J., Grosse-Kunstleve, R. W., Adams, P. D., Winn, M. D., Storoni, L. C., and Read, R. J. (2007) Phaser crystallographic software. *J. Appl. Crystallogr.* **40,** 658–674 CrossRef Medline
40. Emsley, P., and Cowtan, K. (2004) Coot: model-building tools for molecular graphics. *Acta Crystallogr. D Biol. Crystallogr.* **60,** 2126–2132 CrossRef Medline
41. Kovalevskiy, O., Nicholls, R. A., and Murshudov, G. N. (2016) Automated refinement of macromolecular structures at low resolution using prior information. *Acta Crystallogr. D Struct. Biol.* **72,** 1149–1161 CrossRef Medline
42. Murshudov, G. N., Vagin, A. A., and Dodson, E. J. (1997) Refinement of macromolecular structures by the maximum-likelihood method. *Acta Crystallogr. D Biol. Crystallogr.* **53,** 240–255 CrossRef Medline
43. Winn, M. D., Ballard, C. C., Cowtan, K. D., Dodson, E. J., Emsley, P., Evans, P. R., Keegan, R. M., Krissinel, E. B., Leslie, A. G., McCoy, A., McNicholas, S. J., Murshudov, G. N., Pannu, N. S., Potterton, E. A., Powell, H. R., *et al.* (2011) Overview of the CCP4 suite and current developments. *Acta Crystallogr. D Biol. Crystallogr.* **67,** 235–242 CrossRef Medline
44. Adams, P. D., Afonine, P. V., Bunkóczi, G., Chen, V. B., Davis, I. W., Echols, N., Headd, J. J., Hung, L. W., Kapral, G. J., Grosse-Kunstleve, R. W., McCoy, A. J., Moriarty, N. W., Oeffner, R., Read, R. J., Richardson, D. C., *et al.* (2010) PHENIX: a comprehensive Python-based system for macromolecular structure solution. *Acta Crystallogr. D Biol. Crystallogr.* **66,** 213–221 CrossRef Medline
45. Krissinel, E., and Henrick, K. (2007) Inference of macromolecular assemblies from crystalline state. *J. Mol. Biol.* **372,** 774–797 CrossRef Medline
46. Perez-Riverol, Y., Csordas, A., Bai, J., Bernal-Llinares, M., Hewapathirana, S., Kundu, D. J., Inuganti, A., Griss, J., Mayer, G., Eisenacher, M., Pérez, E., Uszkoreit, J., Pfeuffer, J., Sachsenberg, T., Yilmaz, S., *et al.* (2019) The PRIDE database and related tools and resources in 2019: improving support for quantification data. *Nucleic Acids Res.* **47,** D442–D450 CrossRef Medline
47. Tiscornia, G., Singer, O., and Verma, I. M. (2006) Production and purification of lentiviral vectors. *Nat. Protoc.* **1,** 241–245 CrossRef Medline
48. Shevchenko, A., Tomas, H., Havlis, J., Olsen, J. V., and Mann, M. (2006) In-gel digestion for mass spectrometric characterization of proteins and proteomes. *Nat. Protoc.* **1,** 2856–2860 CrossRef Medline
49. Rappsilber, J., Ishihama, Y., and Mann, M. (2003) Stop and go extraction tips for matrix-assisted laser desorption/ionization, nanoelectrospray, and LC/MS sample pretreatment in proteomics. *Anal. Chem.* **75,** 663–670 CrossRef Medline
50. Michalski, A., Damoc, E., Hauschild, J. P., Lange, O., Wieghaus, A., Makarov, A., Nagaraj, N., Cox, J., Mann, M., and Horning, S. (2011) Mass spectrometry-based proteomics using Q Exactive, a high-performance benchtop quadrupole Orbitrap mass spectrometer. *Mol. Cell Proteomics* **10,** M111.011015 CrossRef Medline
51. Cox, J., and Mann, M. (2008) MaxQuant enables high peptide identification rates, individualized p.p.b.-range mass accuracies and proteome-wide protein quantification. *Nat. Biotechnol.* **26,** 1367–1372 CrossRef Medline
52. Cox, J., Neuhauser, N., Michalski, A., Scheltema, R. A., Olsen, J. V., and Mann, M. (2011) Andromeda: a peptide search engine integrated into the MaxQuant environment. *J Proteome Res.* **10,** 1794–1805 CrossRef Medline
53. Cox, J., Hein, M. Y., Luber, C. A., Paron, I., Nagaraj, N., and Mann, M. (2014) Accurate proteome-wide label-free quantification by delayed normalization and maximal peptide ratio extraction, termed MaxLFQ. *Mol. Cell Proteomics* **13,** 2513–2526 CrossRef Medline
54. Tyanova, S., Temu, T., Sinitcyn, P., Carlson, A., Hein, M. Y., Geiger, T., Mann, M., and Cox, J. (2016) The Perseus computational platform for comprehensive analysis of (prote)omics data. *Nat. Methods* **13,** 731–740 CrossRef Medline
55. Sato, T., Stange, D. E., Ferrante, M., Vries, R. G., Van Es, J. H., Van den Brink, S., Van Houdt, W. J., Pronk, A., Van Gorp, J., Siersema, P. D., and Clevers, H. (2011) Long-term expansion of epithelial organoids from human colon, adenoma, adenocarcinoma, and Barrett's epithelium. *Gastroenterology* **141,** 1762–1772 CrossRef Medline
56. Koo, B. K., Stange, D. E., Sato, T., Karthaus, W., Farin, H. F., Huch, M., van Es, J. H., and Clevers, H. (2011) Controlled gene expression in primary Lgr5 organoid cultures. *Nat. Methods* **9,** 81–83 CrossRef Medline